Effect of Li Substitution on the Structure and Dielectric Constant of Bi0.5(Na1-xLix)0.5TiO3 (0 ≤ x ≤ 0.20) Solid Solution Series

K Anjali
National Chemical Laboratory CSIR

T G Ajithkumar
National Chemical Laboratory CSIR

Pattayil Joy (pa.joy@ncl.res.in)
National Chemical Laboratory CSIR https://orcid.org/0000-0003-2125-0976

Research Article

Keywords: Bismuth sodium titanate, Bi0.5Na0.5TiO3, Li substitution, Lead free ferroelectrics, Structure property correlation, Raman spectroscopy, Dielectrics

DOI: https://doi.org/10.21203/rs.3.rs-30901/v1

Abstract

Bismuth sodium titanate $Bi_{0.5}Na_{0.5}TiO_3$ (BNT) is a lead-free piezoelectric ceramic material with high Curie temperature. The effect of substitution of the smaller ion Li^+ for the larger ion Na^+ in $Bi_{0.5}(Na_{1-x}Li_x)_{0.5}TiO_3$ ($0 \leq x \leq 0.20$) on the structure of BNT is studied using powder X-ray diffraction (XRD) and Raman spectroscopy. Rietveld refinement analysis of the powder XRD patterns showed that all the compositions formed under monoclinic Cc space group, with the lattice parameters showing minor changes above $x > 0.08$. Raman spectral parameters such as position and intensity of a peak also showed a similar trend in the same Li concentration range with increasing Li content. A corresponding change in the variation of the dielectric constant with increasing Li content is observed suggesting a close correlation between the local structure and properties of the different compositions in the $Bi_{0.5}(Na_{1-x}Li_x)_{0.5}TiO_3$ solid solution series.

1 Introduction

Bismuth sodium titanate, $Bi_{0.5}Na_{0.5}TiO_3$ (BNT) is a piezoelectric ceramic material with strong ferroelectric properties such as large remnant polarization (P_r = 38 μC/cm^2) and high Curie temperature (T_C = 320 ^{o}C) [1–4]. The main drawbacks of BNT for practical applications are its large coercive field and high electrical conductivity. Several studies have been reported in the literature on the modifications of BNT to overcome these drawbacks and to improve its piezoelectric properties [5–10]. Most of these studies are centered on the substitution of Bi- or Na-site of the perovskite lattice by other metal ions of comparable size, ionic character, etc. Duke *et al* studied the improvement of ionic conductivity in A-site lithium doped sodium bismuth titanate. The optimal doping level of 4 at% Li on the Bi site improves the ionic conductivity by one order of magnitude to ~ 7×10^{-3} S/cm at 600 °C. Comparison with other oxide-ion conductors indicated that Li-doped BNT materials are promising candidates for intermediate temperature SOFC applications [11]. Gao *et al* studied the electric field and composition-dependent behavior of $(Na_{0.484}Bi_{0.456}Ba_{0.06})Ti_{0.97}Nb_{0.03}O_3 - xLi^+$ (x = 0, 0.005, 0.01, 0.015) ceramics and [12]. The introduction of Li cations enhanced the piezoelectric strain with the highest bipolar strain of 0.47% achieved at x = 0.01 at an applied electric field of 70 kV/cm, and the corresponding normalized strain (d_{33}^*) reached up to 671 pm/V. It has been reported that the dielectric and piezoelectric properties are enhanced when Na^+ is replaced by K^+ in $Bi_{0.5}(Na_{1-x}K_x)_{0.5}TiO_3$ solid solution series (BNT-BKT) [13–14]. Lin *et al* studied Li and K co-substituted $Bi_{0.5}(Na_{1-x-y}K_yLi_x)_{0.5}TiO_3$ solid solution series and observed that a small amount of Li^+ substitution improved the sintering characteristics and the piezoelectric properties [15]. The properties of Li^+ and K^+ co-substituted BNT solid solution series have also been studied by other researchers [16–18].

There are few studies reported in the literature on the substitution of Na^+ by Li^+ in BNT. Lu *et al* synthesized $Bi_{0.5}(Na_{1-x}Li_x)_{0.5}TiO_3$ solid solution series by the ceramic method and observed that the compositions in the range $0 \leq x \leq 0.20$ have perovskite structure with rhombohedral symmetry [19]. The maximum piezoelectric constant, d_{33}, and planar electromechanical coupling factor, K_p, are obtained as

110 pC/N and 0.18 at $x = 0.15$, respectively. The un-substituted BNT has a lower piezoelectric coupling constant d_{33}(80 pC/N) and planar electromechanical coupling factor$\mathrm{K_p}$ (0.14). The mechanical quality factor, $\mathrm{Q_m}$, was found to decrease with increasing Li^+ content. Said and Maaoui investigated the dielectric behavior of the $Bi_{0.5}(Na_{1-x}Li_x)_{0.5}TiO_3$ solid solution series and found relaxor-type behavior with a diffuse phase transition for low Li^+ substitution in the range $0 \leq x \leq 0.20$ [20]. The authors explained the relaxor behavior is due to the cation disorder in the A-site of the perovskite lattice.

Detailed structural studies on $Bi_{0.5}(Na_{1-x}Li_x)_{0.5}TiO_3$ or $(1-x)Bi_{0.5}Na_{0.5}TiO_3 – xBi_{0.5}Li_{0.5}TiO_3$ solid solution series are not yet reported. In the present study, a detailed structural characterization of $(1-x)Bi_{0.5}Na_{0.5}TiO_3 – xBi_{0.5}Li_{0.5}TiO_3$, represented as (1-*x*)BNT– *x*BLT, in the range $0 \leq x \leq 0.20$ was carried out using Rietveld analysis of the XRD patterns and Raman spectroscopy and the changes in structure are correlated with the changes in the dielectric properties. Since the ionic size of Li^+ (0.92 Å) is smaller than that of Na^+ (1.39 Å) (values for 8-fold coordination) [21], the substitution of Li^+ for Na^+ in BNT may cause structural changes and phase transition. This is investigated by the Rietveld refinement analysis of the XRD patterns [22] of different close compositions in the (1-*x*)BNT– *x*BLT series. Similarly, local structural changes are studied by Raman spectroscopy. The effect of substitution of Li^+ on the dielectric properties of the solid solutions are also examined to find correlation, if any, with the associated structural changes.

2 Experimental

Solid solutions in the (1-*x*)BNT – *x*BLT series were prepared by a citrate-gel method for *x* ranging from 0 to 0.20 from the corresponding metal nitrates and titanium isopropoxide taken in the required stoichiometric ratio. Bismuth nitrate ($Bi(NO_3)_3.5H_2O$) was dissolved in dilute nitric acid, and sodium nitrate ($NaNO_3$) and lithium nitrate ($LiNO_3$) were dissolved in distilled water. Calculated amount of citric acid was dissolved in a solution of titanium isopropoxide ($Ti[OCH(CH_3)_2]_4$) in isopropyl alcohol by stirring for 30 minutes. The ratio of citric acid to metal nitrate content was taken as 3:1. The individual metal nitrates solutions were mixed together and the mixture was added to the titanium solution with constant stirring and evaporated at 60 ^oC until a transparent viscous gel was obtained. The dried gel was heated at 150 ^oC overnight and crushed to a fine powder. The powder samples were initially heated at 400 ^oC, 850 ^oC and 1000 ^oC with intermediate grinding. The powder samples were uniaxially pressed into circular discs (10 mm diameter x 3 mm height) at a pressure of 8 MPa and sintered at 1150 ^oC for 2 hours. All the samples were sintered under identical conditions with heating and cooling rate of 5 ^oC/min. The samples in the (1-*x*)BNT– *x*BLT series were labeled as BNT ($x = 0$) and *x*BLT.

Structural analysis of the sintered samples was performed by powder X-ray diffraction (XRD) on a PANalytical X'pert PRO powder X-ray diffractometer. Raman spectra were recorded on a Lab RAM HR spectrometer (HORIBA JOBIN YVON, Model No. HR 800) and deconvoluted using the Origin software. The densities of the sintered pellets were measured by the Archimedes method. Dielectric constants of the sintered pellets were measured at room temperature, using an impedance bridge (Model 1608A, General Radio Company) at 1 kHz. The microstructures of the sintered samples were obtained using a scanning

electron microscope (FEI Quanta 200 3D ESEM). Rietveld refinement of the powder XRD patterns was carried out using the software 'General structure analysis System' (GSAS-EXPGUI).

3 Results And Discussion

Figure 1 shows the powder XRD patterns of selected compositions in the solid solution series (1-*x*)BNT–*x*BLT. No additional peaks, other than those from the perovskite phase, are detected in the XRD patterns suggesting the single phase nature of the different compositions. Rietveld refinement analysis of all the studied compositions of (1-*x*)BNT–*x*BLT are carried out using the monoclinic Cc space group. All the compositions gave reasonable good fit with low values for reduced χ^2 and R_p. Table S1 (ESM) gives the results obtained from Rietveld analysis for all the studied compositions in (1-*x*)BNT–*x*BLT ($0 \leq x \leq 0.20$).

Figure 2 shows the variation of the monoclinic lattice parameters *a*, *b*, and *c*, as a function of BLT content in (1-*x*)BNT–*x*BLT. On increasing the BLT concentration, the lattice parameters '*a'* and '*c'* are decreased whereas '*b'* is slightly increased. The ionic radius of Li^+ is 0.92 Å and that of Na^+ is 1.18 Å, for 8–fold coordination [21]. When larger Na^+ is replaced by the smaller ion Li^+, the unit cell volume is decreased (Fig. S1, ESM). The substitution of Li^+ causes contraction of the unit cell, and hence corresponding changes are seen in the lattice parameters. The difference between the magnitudes of the lattice parameters for $x = 0$ and 0.2 in the values of '*a*' and '*c*' is obtained as approximately 0.02 Å. Although the lattice parameter '*b*' showed a small increase, the difference is very small (~ 0.006 Å). The small increase in the value of '*b*' could be due to the reduced distortion or tilting of the TiO_6 octahedra in the unit cell on substitution of smaller Li^+ for larger Na^+.

It is interesting to note that the rates of decrease of the lattice parameters '*a'* and '*c'* are different above and below $x \approx 0.08$. A large decrease in the values of the lattice parameters is observed between $x = 0.08$ and 0.16, above which the lattice parameters remain almost constant. Also, $c \approx a^{1/3}$, for $x > 0.16$. Similarly, the lattice parameter '*b'* remains almost constant up to $x \approx 0.1$ and after this concentration, a small increase is observed up to $x = 0.16$ and *'b'* becomes almost constant again at higher Li^+ concentrations. Similar changes are observed in the variation of the unit cell volume also (Fig. S1, ESM). Since the changes in the lattice parameters are very small with increasing Li content, it may be concluded that there is no major structural phase transformation as observed in the case of (1-*x*)BNT–*x*BKT, where the structure is found to change from monoclinic to tetragonal at higher BKT content [23]. The small change in the variation of the lattice parameters around $x \approx 0.1$ may be due to the local structural changes, arising from the inhomogeneous distribution of the substituted Li ions in the lattice for $x < 0.1$. However, onset of a structural phase transition cannot be ruled out in this compositional region, even though good fits are obtained in the Rietveld refinement analysis, using the monoclinic structure in the entire compositional region studied. The fact that the lattice parameters become almost constant for $x > 0.16$ and all three lattice parameters show a major change in the compositional region $0.08 \leq x \leq 0.16$ suggest a probable structural phase transition. If this is true, the compositional region $0.08 \leq x \leq 0.16$ is

likely to belong to a morphotropic phase boundary (MPB) region, as observed in the case of (1-*x*)BNT–*x*BKT [23].

Raman spectra of all the studied compositions are recorded and the changes in the Raman spectra as a function of composition in the BNT – BLT series are studied to get more insights in to the local structural changes with Li substitution. Raman spectra of different compositions of the (1-*x*)BNT–*x*BLT series, after baseline correction, are shown in Fig. 3. Raman spectra of BNT is similar to that already reported in the literature [24–29]. As observed in the case of the BNT–BKT series [24–25], the Raman spectra of the BNT–BLT solid solutions consist of three different regions. The band below 200 cm^{-1} is due to the A-O vibrations in the ABO_3 perovskite lattice, and in the present case it is likely to be due to Bi-O, Na-O and Li-O vibrations. The band observed in the 200–400 cm^{-1} region in the Raman spectra belongs to the Ti-O vibrations and the band in the 400–800 cm^{-1} region belongs to the vibration of the TiO_6 octahedra [24].

If the substitution of smaller Li^+ ion for larger Na^+ in the BNT lattice causes contraction of the unit cell volume and local structural distortions, corresponding signatures are expected in the Raman spectra of the BNT–BLT solid solutions. The immediate observation from the Raman spectra, shown in Fig. 3, is the decrease in the area and the downward frequency shift of the band centered at ~ 135 cm^{-1}. In the case of BNT–BKT solid solution series, an additional band was observed in the 200–400 cm^{-1} region which gave clear indication about the symmetry changes and phase transition [24]. Such prominent changes are not observed in the 200–400 cm^{-1} and 400–800 cm^{-1} regions in the Raman spectra of the BNT–BLT solid solutions. Detailed analysis of the Raman spectra is carried out by the deconvolution of each spectrum and the changes in the parameters are studied.

Raman spectra of the different BNT–BLT compositions are deconvoluted in to seven Gaussian peaks, after normalizing with respect to the intensity of the band in the 200–400 cm^{-1} region. Figure 4 shows the deconvoluted Raman spectra of selected compositions, $x = 0$, 0.04, 0.08, 0.12, 0.16, and 0.20 in the (1-*x*)BNT–*x*BLT solid solution series. The band below 200 cm^{-1} is fitted with one peak. The broad bands in the 200–400 cm^{-1} and 400–800 cm^{-1} regions are deconvoluted in to three peaks each. A small shift in the position of the A – O band of the BNT–BLT solid solutions is observed on Li^+ substitution, with a small increase in the position of the band up to $x \approx 0.1$ and a large decrease above this composition (Fig. S2, ESM). However, the area under the peak is found to decrease almost linearly with increasing Li content (Fig. S2). The band below 200 cm^{-1} belongs to the Na – O/Li – O vibration since the Bi – O band cannot be observed in this frequency region due to the higher mass of the Bi^{3+} ion [25]. The variations in the peak position and area of the band are due the local structural changes due to Li^+ substitution and the low frequency shift may be due to the diffusion of the smaller Li^+ ions in the crystal lattice which will weaken the Li – O bond strength and results in some local symmetry changes.

As mentioned, the Raman band in the 200–400 cm^{-1} region is due to the Ti-O vibrations. Figure 5 shows the variation of the position of the individual peaks in the 200–400 cm^{-1} region with increasing concentration of BLT. On increasing the BLT concentration, the first two components show an upward

frequency shift whereas the third component shows a different trend. For the first two peaks within this band, the positions of the peaks remain almost the same for $x < 0.08$ and $x > 0.12$, with a drastic increase between $x = 0.08$ and 0.12. Similar changes are observed in the case of the third peak also, except for a large drop for $0.08 \leq x \leq 0.12$. Figure 6 shows the changes in total area under the band and the area under the individual peaks of the band in the 200–400 cm^{-1} region with increasing Li content. The area under the individual peaks also show a major change between $x = 0.08$ and $x = 0.12$ as in the case of the changes in the peak positions.

Changes are also observed in the positions of the individual peaks of the Raman band in the 400–800 cm^{-1} region due to the vibration of the TiO_6 octahedra. A linear increase in the position of the individual peaks is observed on increasing the BLT concentration (Fig. S3, ESM). The total area and the areas under the first two peaks are increased whereas the area of the third peak is decreased with increasing BLT concentration (Fig. S4, ESM). Even though the total area increased almost linearly with increasing BLT concentration, the changes in the area of the individual peaks showed different trends below and above $x = 0.08$. The area of peak 1 is independent of x for $x < 0.08$ and then increased with x, area of peak 2 increased up to $x = 0.8$ and then remained almost constant, and area of peak 3 decreased up to $x = 0.08$ and then remained almost constant at higher x.

Thus, the changes in the parameters of the Raman spectra for the bands in the 200–400 cm^{-1} and 400–800 cm^{-1} regions suggest minor changes in the Ti-O bond length and some associated changes in the distortion of the TiO_6 octahedra with partial substitution of Li^+ for Na^+ in $Bi_{0.5}Na_{0.5}TiO_3$. Results from the XRD studies suggested minor structural changes above $x = 0.08$ in (1-x)BNT-xBKT and the Raman studies suggest that this is due to the minor changes in the coordination environment at the A- and B-sites in the perovskite lattice. Hence, corresponding changes in the ferroelectric polarization is expected which may lead to variations in the dielectric constant.

The dielectric constant of all the studied compositions of (1-x)BNT–xBLT, measured at 1 kHz, as a function of BLT concentration is shown in Fig. 7. The dielectric constant shows a small increase up to $x = 0.08$ which is shown in the inset of Fig. 7 and an abrupt change in the slope is observed above $x = 0.08$. For $x \geq 0.12$, the dielectric constant remains almost constant. The maximum dielectric constant observed for the BNT–BLT compositions is \tilde 420. However this value is relatively small, when compared to the maximum dielectric constant observed for the BNT–BKT series which is \tilde 1800 [23]. For the BNT–BKT system, maximum dielectric constant is observed in the MPB region where the monoclinic and tetragonal phases co-exist. Such a phase transition and MPB region is not observed in the case of the BNT–BLT system. Also, the distortion of the monoclinic structure is relatively larger for the BNT–BKT system due to the larger size of the K^+ ions. The observed dielectric constants of the different compositions of the BNT–BLT ceramics are relatively low when compared to the previous literature reports [19–20]. Lu *et al* reported a dielectric constant ~800 for the $x = 0.20$ composition in the BNT–BLT series [19]. This is mainly due to the difference in the synthesis methods, processing conditions, density, sintering temperature and the pressure used for the compaction of pellets.

Figure 8 shows a comparison of the variations in the lattice parameter '*b*', area under the first component of the Raman band in the 200–400 cm^{-1} region and the dielectric constant of the solid solutions with increasing BLT concentration. The Raman band belongs to the Ti-O vibrations in the BNT–BLT solid solution. All the three parameters show similar variation, where the parameters are not much changed till $x \approx 0.08$, a large increase is observed up to $x = 0.12$ and again the parameters remain independent of x in the range $0.12 \leq x \leq 0.20$. Since the Raman parameter reflects the changes in the Ti-O bond with Li^+ substitution, and a similar trend is followed by the lattice parameter '*b*' as well as the dielectric constant, it may be concluded that the changes in the local symmetry contributed to the variations in the dielectric constant with the substitution of Li^+ for Na + in $Bi_{0.5}Na_{0.5}TiO_3$

4 Conclusions

Solid solutions in the series $(1-x)Bi_{0.5}Na_{0.5}TiO_3 - xBi_{0.5}Li_{0.5}TiO_3$, represented as (1-*x*)BNT–*x*BLT, in the range $0 \leq x \leq 0.20$ are studied to understand the effect of substitution of Na by Li in $Bi_{0.5}Na_{0.5}TiO_3$. Rietveld refinement analysis of the XRD patterns suggested small structural distortion and local symmetry changes in the crystal lattice. Raman spectroscopy analysis supported the results obtained from the XRD studies. The changes in the Raman parameters with substitution followed the same trend as that observed in the case of the unit cell parameters. Variation of the structural as well as Raman spectral parameters and the dielectric constant showed similar changes with increasing Li concentration, suggesting a close correlation between the structure and properties of the compositions.

Declarations

Acknowledgments

K. Anjali is grateful to University Grants Commission (UGC), India, for a research fellowship.

References

1. Smolensky GA, Isupov VA, Agranovskaya AI, *et al*. New ferroelectrics of complex composition. *Sov Phys Solid State* 1961, **2**: 2651.
2. Smolenskii GA. Physical phenomena in ferroelectrics with diffused phase transitions. *Jpn J Phys Soc* 1970, **28**: 26.
3. Hiruma Y, Nagata H, Takenaka T. Phase diagram and electrical properties of $Bi_{1/2}Na_{1/2}TiO_3$-based solid solutions. *J Appl Phys* 2008, **104**: 124106.
4. Schutz D, Deluca M, Krauss W, *et al.* Lone-pair-induced covalency as the cause of temperature and field-induced instabilities in bismuth sodium titanate. *Adv Funct Mater* 2012, **22**: 2285.
5. Takenaka T, Sakata K. Dielectric, piezoelectric and pyroelectric properties of $Bi_{1/2}Na_{1/2}TiO_3$-based ceramics. *Ferroelectrics* 1989, **95**: 153.

6. Takenaka T, Maruyama K, Sakata K. $(Bi_{1/2}Na_{1/2})TiO_3$-$BaTiO_3$ system for lead-free piezoelectric ceramics. *Jpn J Appl Phys* 1991, **30**: 2236.
7. Liu X , Zhao Y, Shi J, *et al*. Improvement of dielectric and ferroelectric properties in bismuth sodium titanate based relaxors through Bi non-stoichiometry. *J Alloys Compd* 2019, **799**: 231-238.
8. Ishchuk VM, Gusakova LG, Kisel NG, *et al.* B-site substituted solid solutions on the base of sodium-bismuth titanate. *J Adv Dielectr* 2016, **6**: 1650027.
9. Mohanty HS, Kumar A, Sahoo B, *et al*. Impedance spectroscopic study on microwave sintered (1-x)$Na_{0.5}Bi_{0.5}TiO_3$–xBaTiO3 ceramics. *J Mater Sci: Mater Electron* 2018, **29**: 6966-6977.
10. Zhao Z-H, Gey R-F, Dai Y. Large electro-strain signal of the BNT–BT–KNN lead-free piezoelectric ceramics with CuO doping. *J Adv Dielectr* 2019, **9**: 1950022.
11. Shih DPC, Aguadero A, Skinner SJ. Improvement of ionic conductivity in A-site lithium doped sodium bismuth titanate. *Solid State Ion* 2018, **317**: 32-38.
12. Gao S, Yao Z, Ning L, *et al*. Enhanced Bipolar Strain Response in Lithium/Niobium Co-Doped Sodium–Barium Bismuth Titanate Lead-Free Ceramics. *Adv Eng Mater* 2017, **00**: 1700125.
13. Sasaki A, Chiba T, Mamiya Y, *et al*. Dielectric and piezoelectric properties of $Bi_{0:5}Na_{0:5}TiO_3$-$Bi_{0:5}K_{0:5}TiO_3$ systems. *Jpn J Appl Phys* 1999, **38**: 5564.
14. Moosavi A, Bahrevar MA, Aghaei AR, *et al*. High-field electromechanical response of $Bi_{0:5}Na_{0:5}TiO_3$-$Bi_{0:5}K_{0:5}TiO_3$ across its morphotropic phase boundary. *J Phys D: Appl Phys* 2014, **47**: 055304.
15. Lin D, Xiao D, Zhu J, *et al*. Synthesis and piezoelectric properties of lead-free piezoelectric $[Bi_{0.5}(Na_{1-x-y}K_xLi_y)_{0.5}]TiO_3$ ceramic. *Mater Lett* 2004, **58**: 615–618.
16. Lu W, Wang Y, Fan G, *et al*. The structural and electrical properties of Li and K substituted $Bi_{0.5}Na_{0.5}TiO_3$ ferroelectric ceramics. *J Alloys Compd* 2011, **509**: 2738–2744.
17. Lin D, Zheng Q, Xu C, *et al*. Structure, electrical properties and temperature characteristics of $Bi_{0.5}Na_{0.5}TiO_3$–$Bi_{0.5}K_{0.5}TiO_3$–$Bi_{0.5}Li_{0.5}TiO_3$ lead-free piezoelectric ceramics. *Appl Phys A* 2008, **93**: 549–558.
18. Ming B-Q, Wang J-F, Zang G-Z. Effects of Li Substitution and Sintering Temperature on Properties of $Bi_{0.5}(Na, K)_{0.5}TiO_3$ Lead-Free Piezoelectric Ceramics. *Chin Phys Lett* 2008, **25**: 3776.
19. Lu W, Fan G, Wang X, *et al*. Dielectric and Piezoelectric Properties of $[Bi_{0.5}(Na_{1-x}Li_x)_{0:5}]TiO_3$ Lead-Free Ceramics. *Jpn J Appl Phys* 2006, **45**: 8763–8765.
20. Said S, Maaoui ME. Relaxor behavior in the Perovskite-type $Bi_{0.5}(Na_{1-x}Li_x)_{0.5}TiO_3$ ($0 \leq x \geq 0.2$) solid solution. *J Electroceram* 2015, **35**: 90-97.
21. Shannon RD. Revised effective ionic radii and systematic studies of interatomic distances in halides and chalcogenides. *Acta Cryst A* 1976, **32**: 77671.
22. Toby B. EXPGUI, a graphical user interface for GSAS. *J Appl Crystallogr* 2001, **34**: 210-213.
23. Anjali K, Ajithkumar TG, Joy PA. Correlations between structure, microstructure, density and dielectric properties of the lead–free ferroelectrics $Bi_{0.5}(Na,K)_{0.5}TiO_3$. J Adv Dielectr 2015, **5**: 1550028.

24. Anjali K, Ajithkumar TG, Joy PA. Raman and ^{23}Na solid-state NMR studies on the lead-free ferroelectrics $Bi_{0.5}(Na_{1-x}K_x)_{0.5}TiO_3$ in the morphotropic phase boundary region. *Mater Res Bull* 2019, **118**: 110506.
25. Kreisel J, Glazer AM, Jones G, *et al*. An X-ray diffraction and Raman spectroscopy investigation of A–site substituted perovskite compounds: the $(Na_{1-x}K_x)_{0.5}Bi_{0.5}TiO_3$ ($0 \leq x \leq 1$) solid solution. *J Phys Condens Matter* 2000, **12**: 3267.
26. Zhang M-S, Scott JF, Zvirgzds JA. Raman spectroscopy of $Na_{0.5}Bi_{0.5}TiO_3$. *Ferroelectr Lett Sect* 1986, **6**: 147–152.
27. Siny IG, Husson E, Beny JM, *et al*. Raman scattering in the relaxor-type ferroelectric $Na_{1/2}Bi_{1/2}TiO_3$. *Ferroelectrics* 2000, **248**: 57–78.
28. Siny IG, Smirnova TA, Kruzina TV. The phase transition dynamics in $Na_{½}Bi_{½}TiO_3$. *Ferroelectrics* 1991, **124**: 207–212.
29. Xie H, Jin L, Shen D, *et al*. Morphotropic phase boundary, segregation effect and crystal growth in the NBT–KBT system. *J Cryst Growth* 2009, **311**: 3626–3630.

Figures

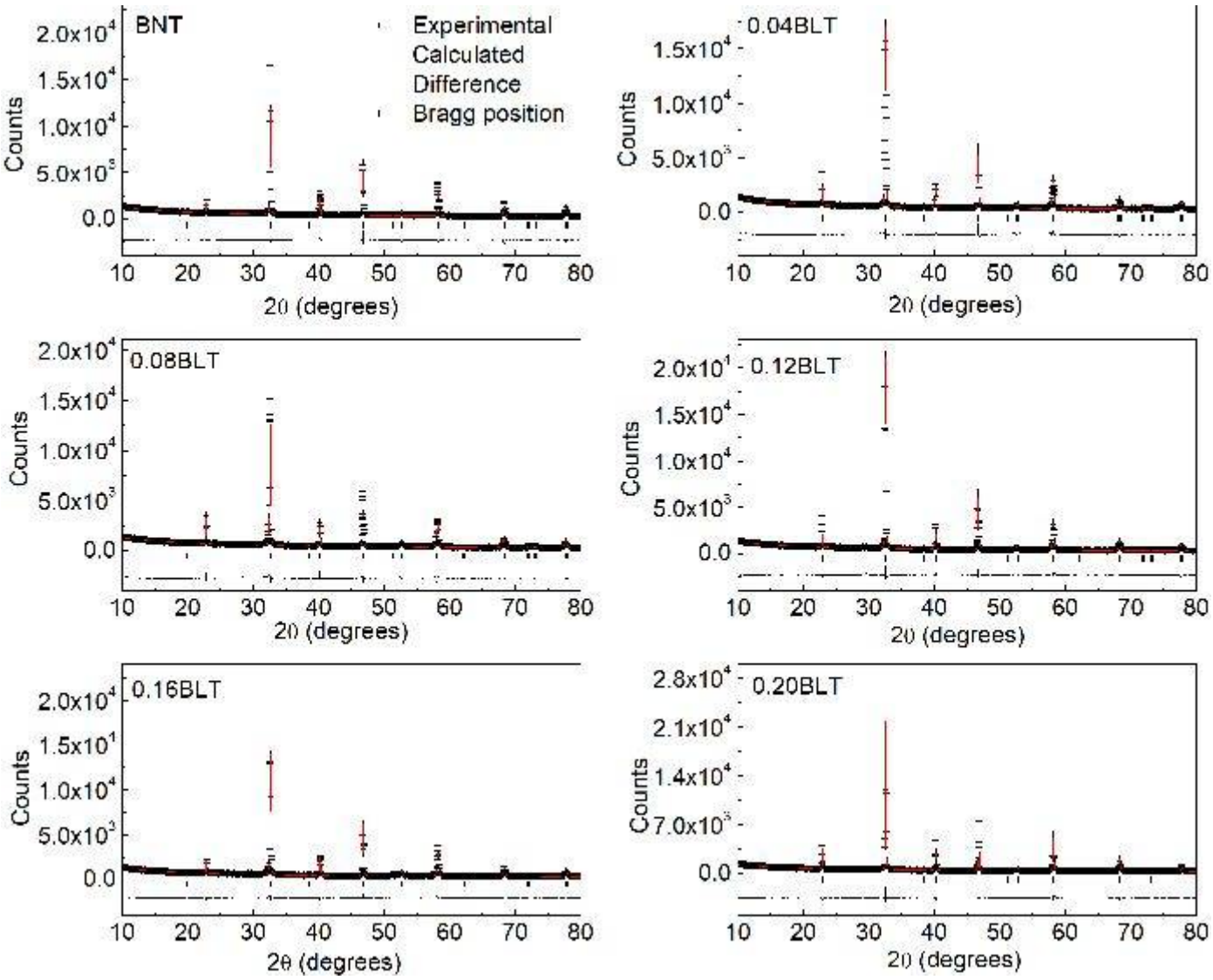

Figure 1

Results of the Rietveld refinement analysis of (1-x)BNT–xBLT using the monoclinic Cc space group, for x = 0, 0.04, 0.08, 0.12, 0.16, and 0.20.

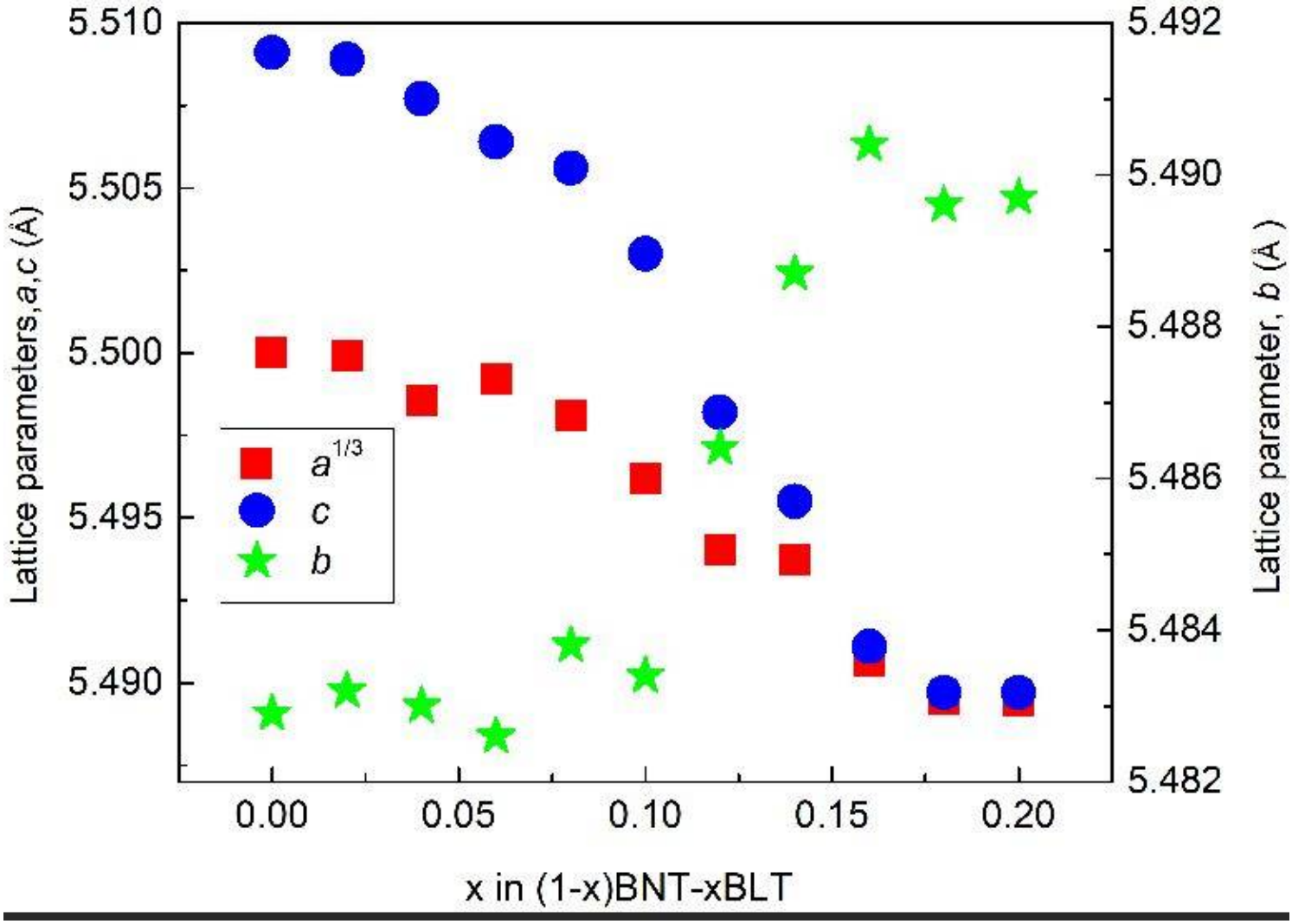

Figure 2

Variation of monoclinic lattice parameters of (1-x)BNT–xBLT solid solution series as a function of x.

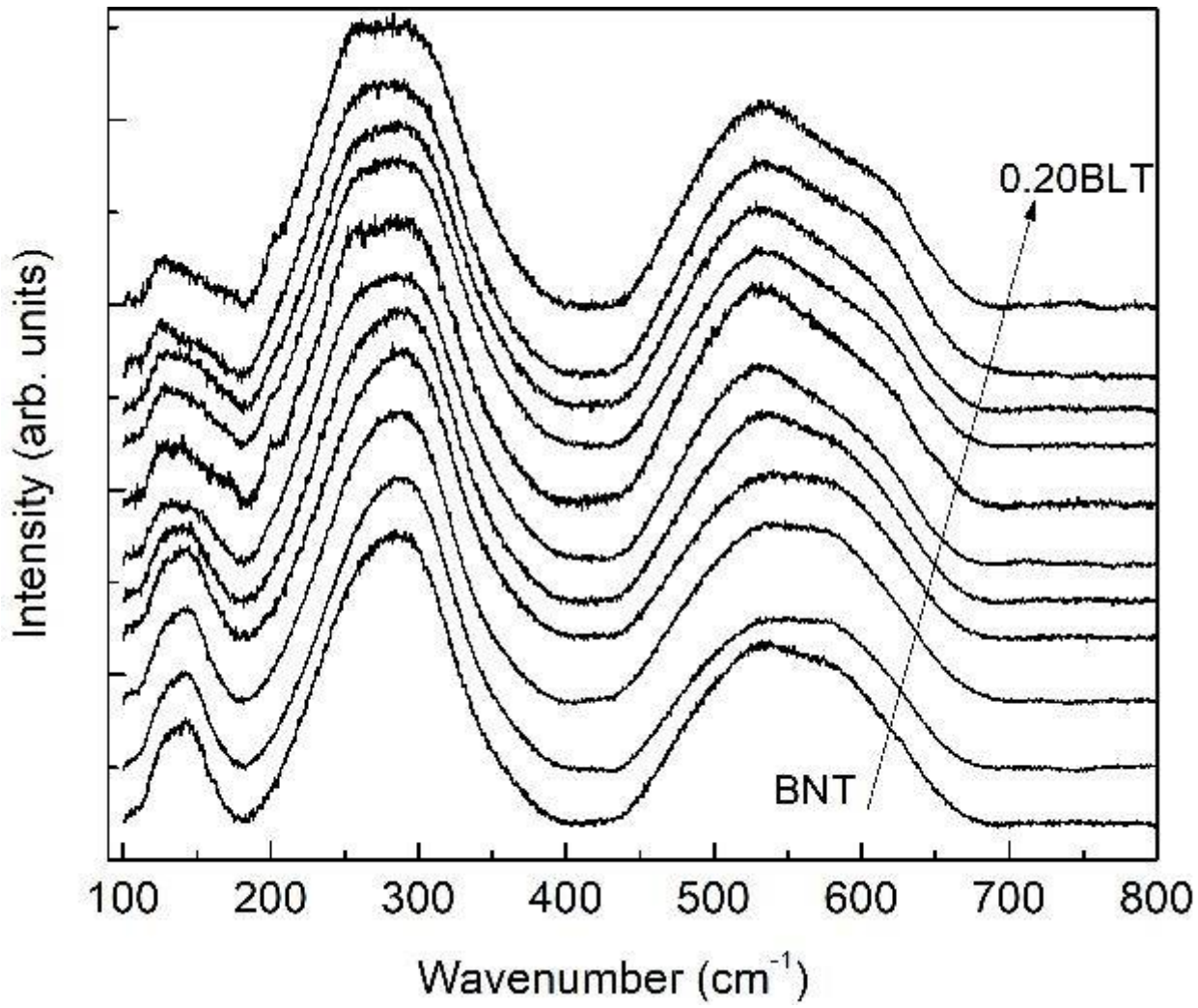

Figure 3

Raman spectra of different compositions in (1-x)BNT–xBLT for $0 \leq x \leq 0.20$ ($\Delta x = 0.02$).

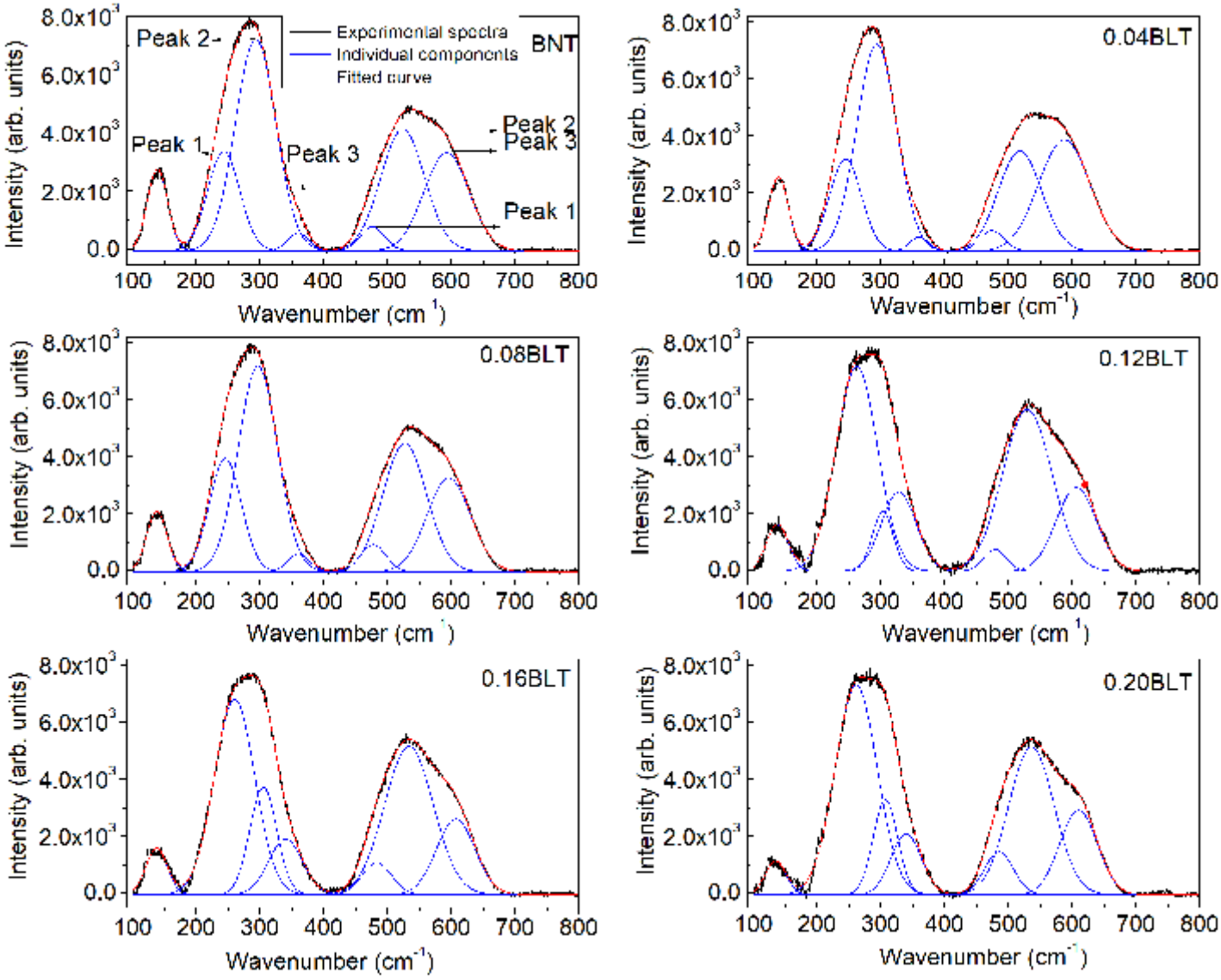

Figure 4

Deconvoluted Raman spectra of selected compositions in (1-x)BNT–xBLT. The black, red and blue curves correspond to experimental spectra, fitted curve and the individual components, respectively.

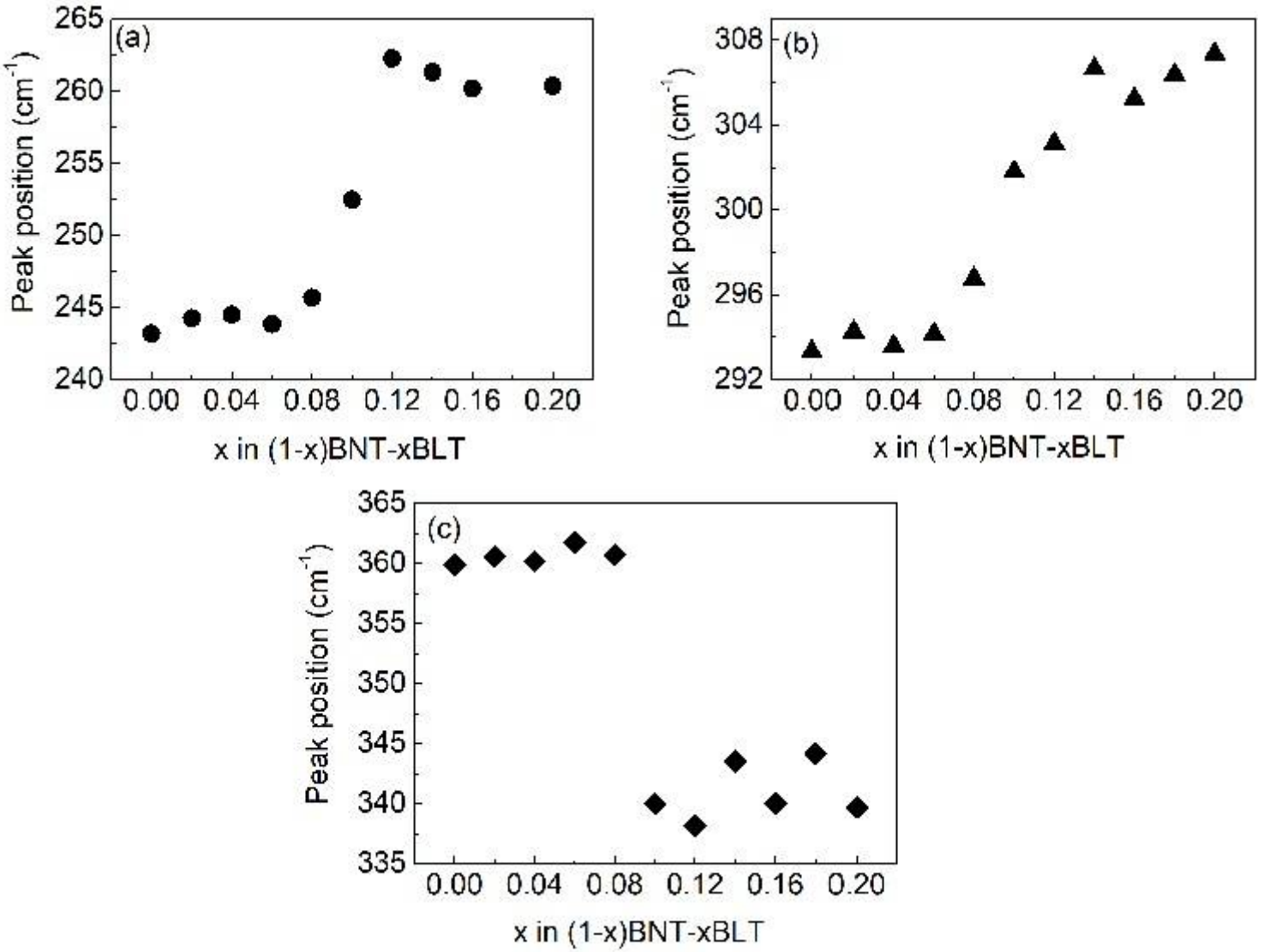

Figure 5

Changes in the individual peak positions of the Raman band in the 200□400 cm-1 region as a function of x in (1-x)BNT–xBLT. (a) 1st peak, (b) 2nd peak, and (c) 3rd peak as defined in figure 4.

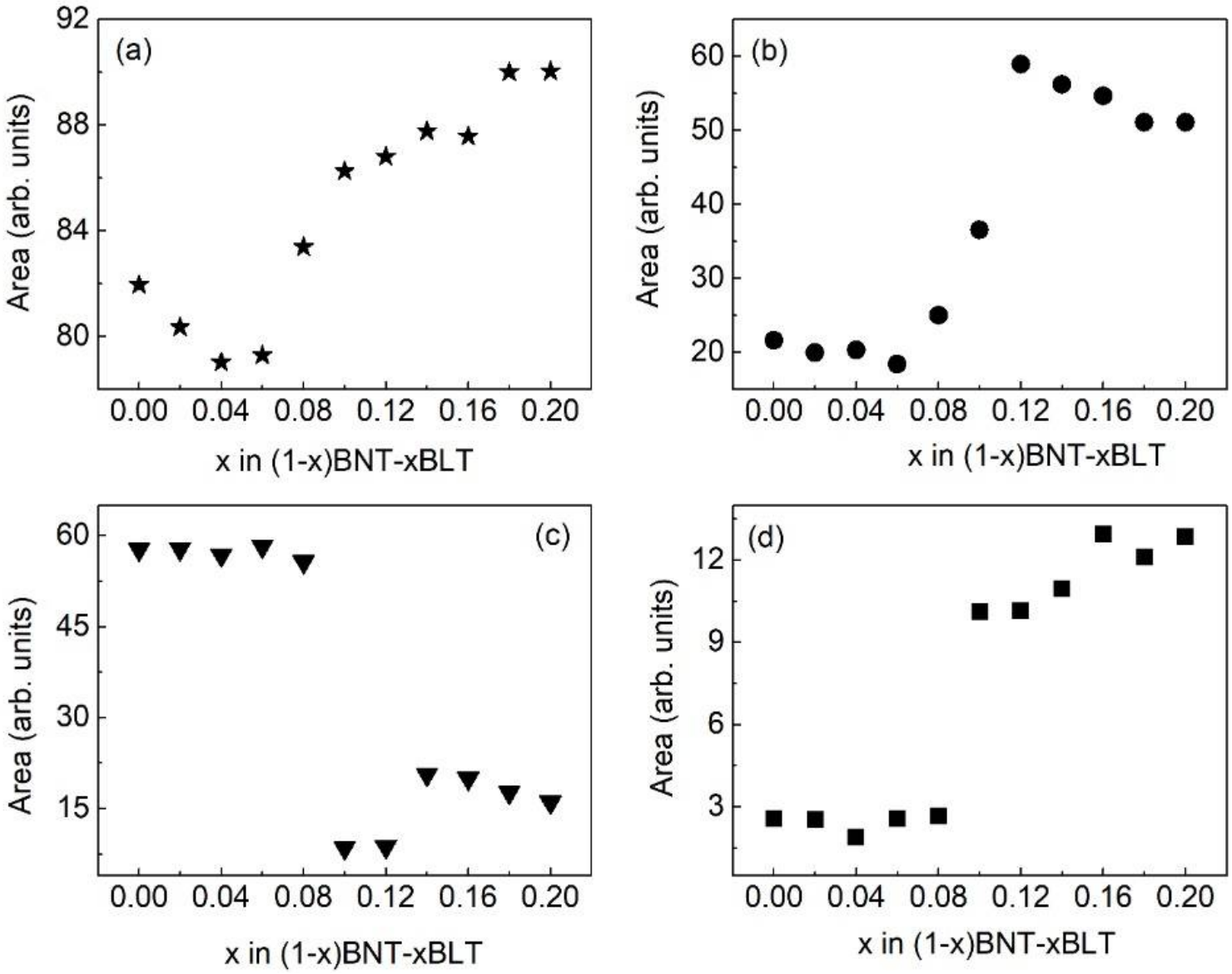

Figure 6

(a) Total area, and (b) area under the 1st peak, (c) area under the 2nd peak, and (d) area under the 3rd peak (as defined in figure 4) of the Raman band in the 200–400 cm-1 region as a function of x in (1-x)BNT–xBLT.

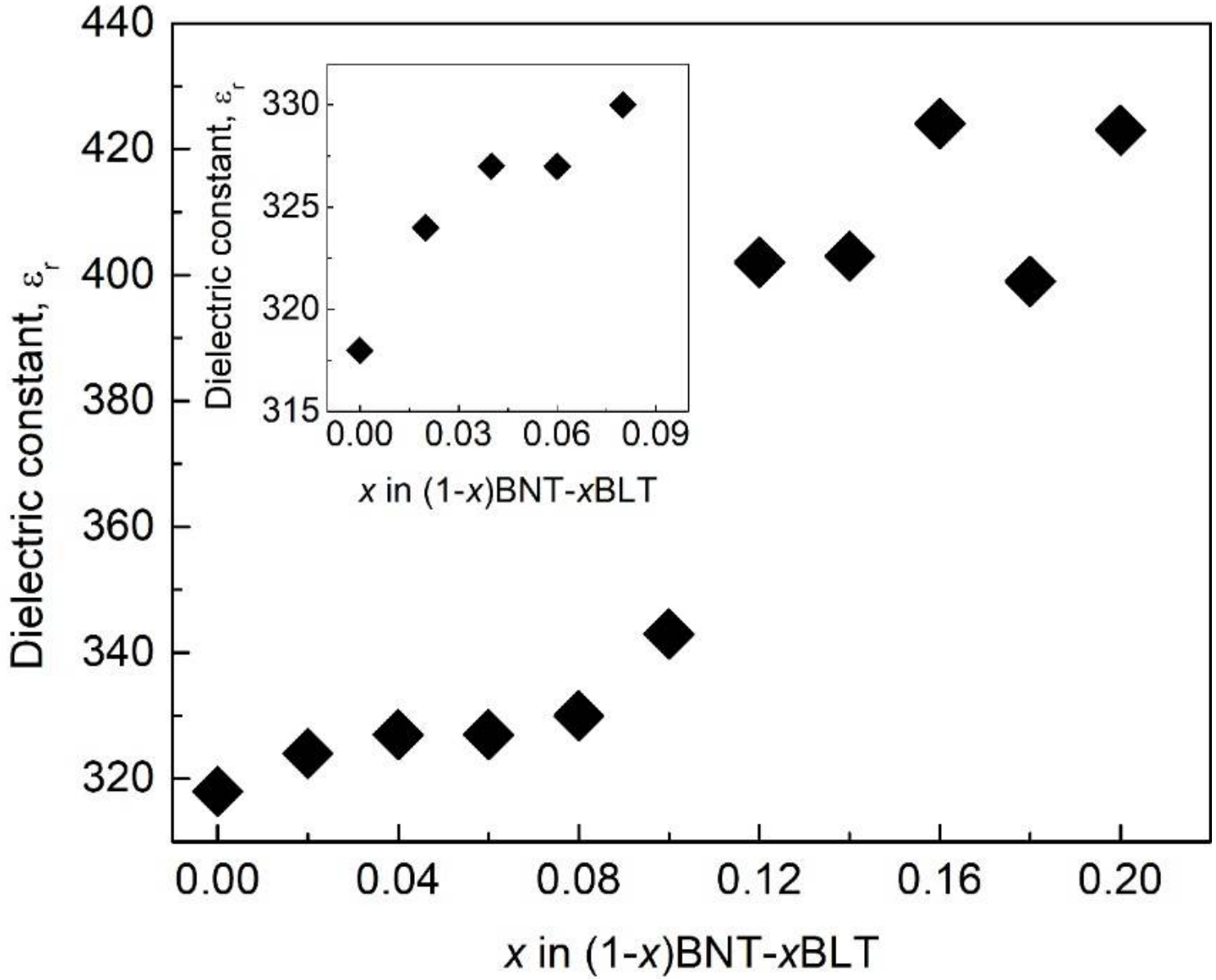

Figure 7

Variation of the dielectric constant of (1-x)BNT–xBLT as a function of x; inset showing zoomed graph for $0 \leq x \leq 0.1$.

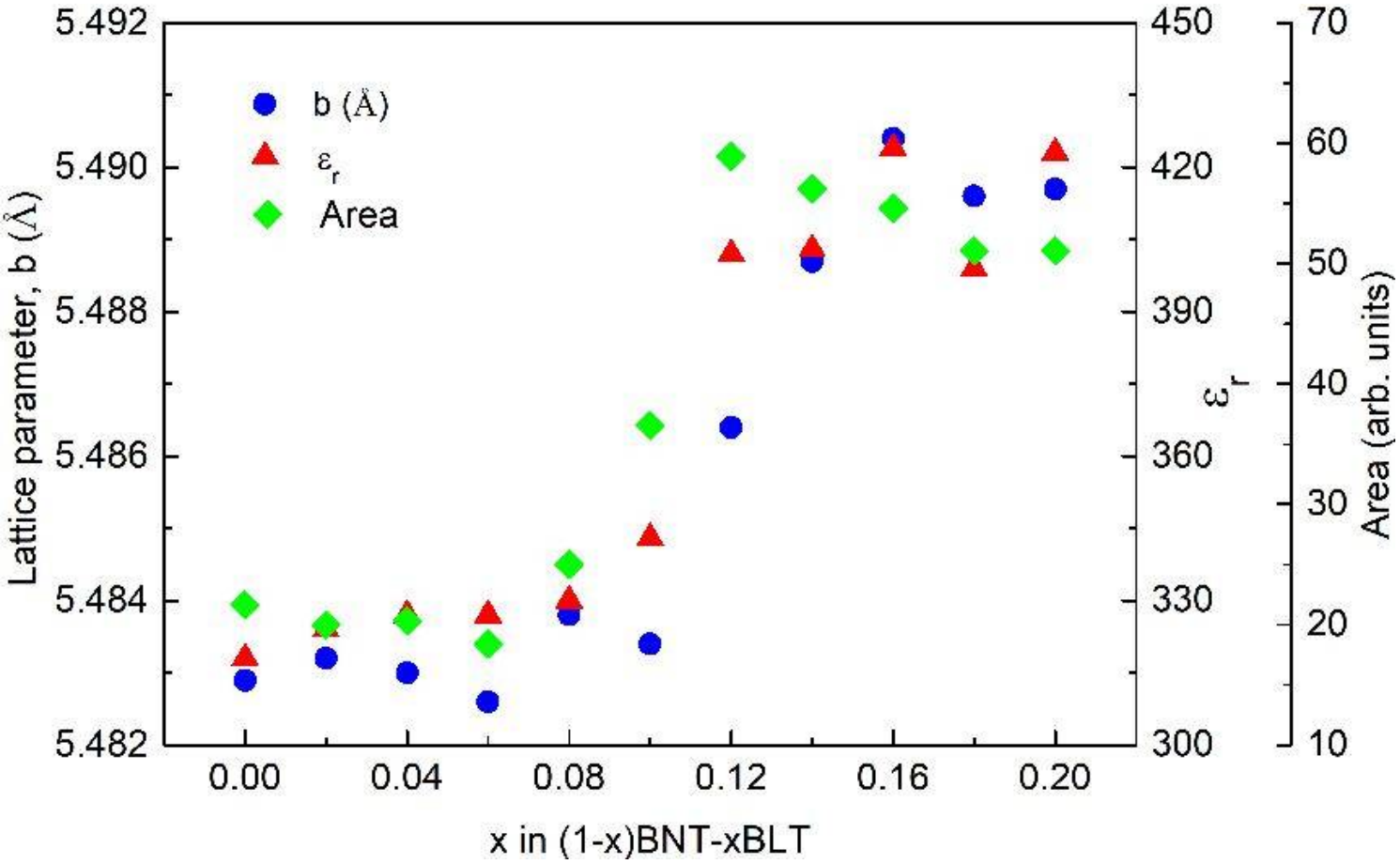

Figure 8

Comparison of the lattice parameter ‘b’, dielectric constant (εr) and area under the first peak of the Raman band in the 200-400 cm-1 region, as a function of x in the (1-x)BNT-xBLT series.

Supplementary Files

This is a list of supplementary files associated with this preprint. Click to download.

- BNTBLTSI.docx